ACS Energy LETTERS

http://pubs.acs.org/journal/aelccp

FOCUS REVIEW

Leveraging Low-Energy Structural Thermodynamics in Halide Perovskites

Bryan A. Rosales, Kelly Schutt, Joseph J. Berry, and Lance M. Wheeler*

Cite This: *ACS Energy Lett.* 2023, 8, 1705−1715

Read Online

ACCESS | Metrics & More | Article Recommendations | Supporting Information

ABSTRACT: **Metal halide perovskites (MHPs) combine extraordinary optoelectronic properties with chemical and mechanical properties not found in their semiconductor counterparts. For instance, they exhibit optoelectronic properties on par with single-crystalline gallium arsenide yet exhibit near-zero formation energies. The small lattice energy of MHPs means they undergo a rich diversity of polymorphism near standard conditions like organic materials. MHPs also demonstrate ionic transport as high as state-of-the-art battery electrodes. The most widespread applications for metal halide perovskites (e.g., photovoltaics and solid-state lighting) typically view low formation energies, polymorphism, and high ion transport as a nuisance that should be eliminated. Here, we put these properties into perspective by comparing them to other technologically relevant semiconductors to highlight how unique this combination of properties are for semiconductors and to illustrate ways to leverage these properties in emerging applications.**

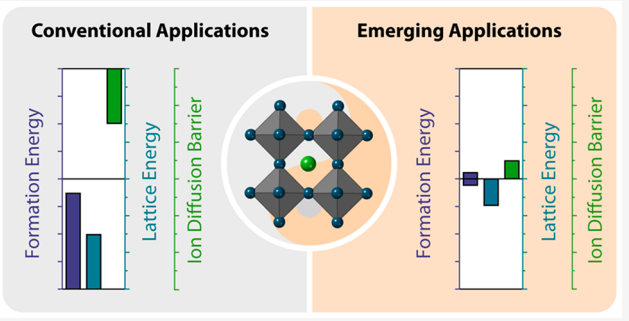

Metal halide perovskites (MHPs) exhibit outstanding optoelectronic properties[1] featuring long carrier lifetimes and diffusion lengths, tunable bandgaps, and exceptional defect tolerance[2,3] that result from a crystalline-like electronic band structure combined with liquid-like ionic lattices.[4] The prototypical MHP structure is represented by AMX_3 (A = methylammonium (MA^+), formamidinium (FA^+), Cs^+, etc.; M = Pb^{2+}, Sn^{2+}; X = I^-, Br^-, Cl^-), characterized by a 3D network of interconnected $[MX_6]^{4-}$ octahedra with monovalent A-site cations occupying interstitial sites (Figure 1). The connectivity of the $[MX_6]^{4-}$ octahedra dictates the observed optoelectronic properties and can range from the fully connected perovskite phase (3D) to partially connected (2D/1D) and fully isolated (0D) non-perovskite phases.[5] MHPs also accommodate a variety of dopants that influence the optoelectronic properties by disrupting the $[MX_6]^{4-}$ octahedral network and by interacting with the soft, polarizable lattice. However, doping mechanisms and lattice incorporation of dopants in MHPs are far from fully understood and remain an area of active investigation.[6]

MHPs undergo a variety of structural changes near standard optoelectronic device operational conditions. Though MHP-based photovoltaic (PV) devices have achieved a remarkable >25% power conversion efficiency (PCE) within a decade of research,[7] fundamental material properties are easily changed by exposure to humidity, heat, electric fields, and light, which, if not managed, result in undesirable transitions between crystal structures, changes in electronic structure, ion migration, and irreversible decomposition.[8−10] Transformation of material properties is detrimental to many established applications of MHPs spanning PVs, electronics, light-emitting diodes (LEDs), lasers, and thermoelectrics (Figure 1). Considerable effort has gone into improving and managing transformations in MHPs to prevent changes in crystalline or electronic structure through formation energy manipulation,[11−13] reducing defect density,[14] and incorporating hydrophobic organic cations.[15]

In MHP literature, "stability" generally refers to resilience to changes in material properties, and numerous methods to improve stability have been highlighted in many literature reviews.[8,28] A recent review surveyed applications that exploit MHP instability.[29] Here, we begin with the fundamental properties of MHP materials that underpin stability by comparing the formation energy, lattice energy, and ionic transport of MHP materials to other technologically relevant semiconductors before turning to novel applications that exploit MHP instabilities. Our analysis illuminates just how

Received: November 27, 2022
Accepted: February 13, 2023
Published: March 9, 2023

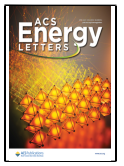

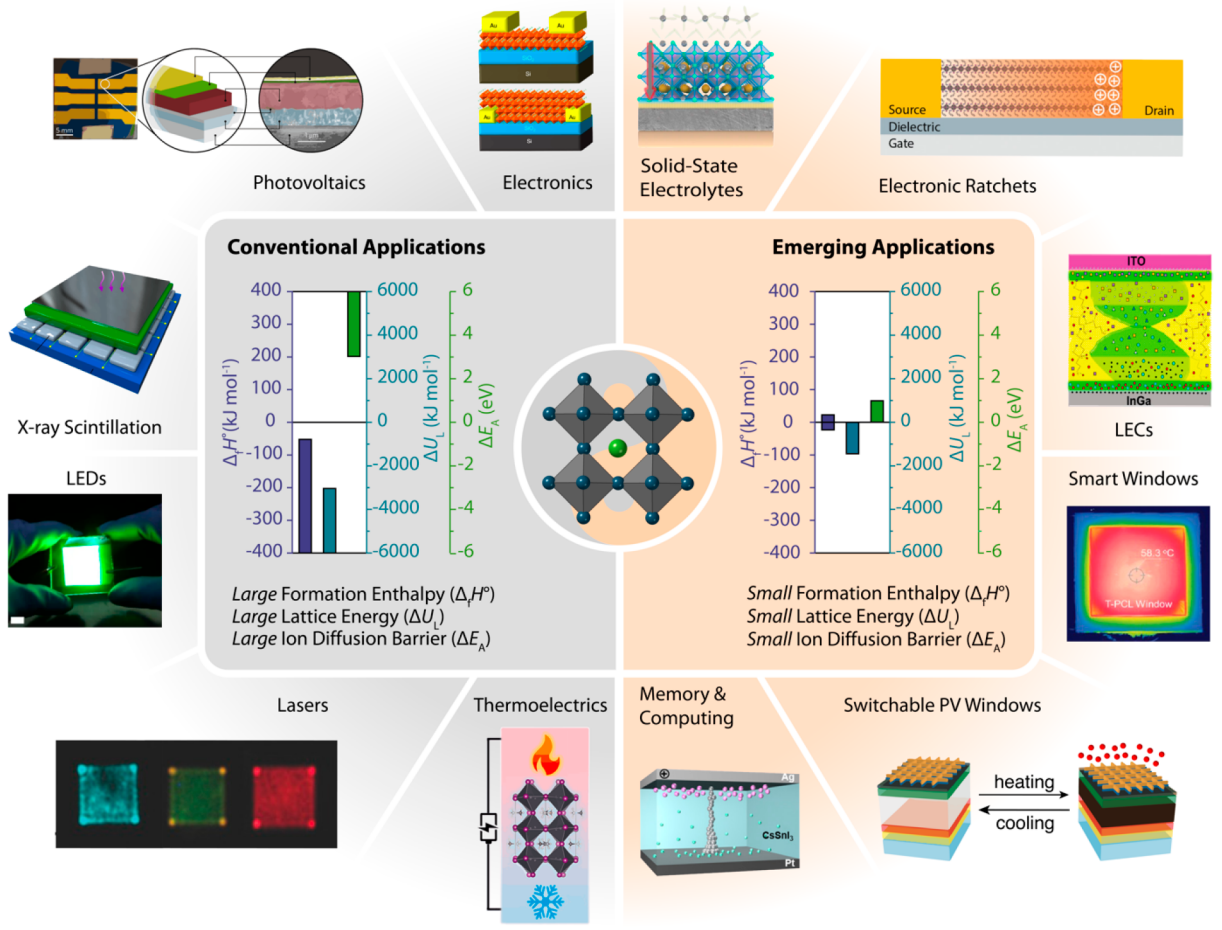

Figure 1. Schematic overview comparing conventional MHP applications that require high resilience to material property transformations with emerging MHP applications that take advantage of material property transformations. X-ray scintillation image adapted from ref 16, Springer Nature 2018. Electronics image adapted from ref 17, Springer Nature 2018. CC-BY: https://creativecommons.org/licenses/by/4.0/. LEDs image adapted from ref 18, Springer Nature 2021. Photovoltaics image adapted from ref 19, Springer Nature 2018. Solid-state electrolytes image adapted from ref 20, Springer Nature 2020. CC-BY: https://creativecommons.org/licenses/by/4.0/. Switchable PV windows image adapted from ref 21, Springer Nature 2017. CC-BY: https://creativecommons.org/licenses/by/4.0/. Smart windows image adapted from ref 22, Wiley-VCH 2022. CC-BY: https://creativecommons.org/licenses/by/4.0/. Lasers image adapted from ref 23, Wiley 2016. Electronic ratchets image adapted from ref 24, Wiley-VCH 2020. LECs image adapted from ref 25, Wiley-VCH 2020. CC-BY: https://creativecommons.org/licenses/by/4.0/. Thermoelectrics image adapted from ref 26, American Chemical Society 2021. Memory & Computing image adapted from ref 27, American Chemical Society 2019.

> Our analysis illuminates just how unique MHP structural properties are across materials science.

unique MHP structural properties are across materials science. Instead of the stabilization-centric narrative driven by PV literature, we highlight MHPs as switchable and stimuli-responsive semiconductors[29] that enable new applications spanning switchable PV smart windows,[21,30] electronic ratchets,[24] solid-state electrolytes,[20] light-emitting electrochemical cells (LECs),[25] and next-generation memory or neuromorphic computing elements[27,31,32] (Figure 1).

Formation Energy of MHPs. Unlike traditional semiconductors, MHPs are entirely solution processable at low temperatures and atmospheric pressure,[10,33] and do not require high-temperature melt-processing, vapor phase growth in a UHV chamber, or forming inks from nanocrystals that were presynthesized at higher temperatures. MHP single crystals can also be synthesized at room temperature,[34] and engineering the acidity of the growth solution enables low temperature growth with reduced defect densities.[35] In contrast to MHPs, conventional semiconductors such as Si are grown by heating above their melting point of 1414 °C while III−V semiconductors require vapor phase growth above 550 °C in ultrahigh vacuum.[36] Low energy intensity processing promises reduced fabrication costs and increased manufacturing throughput for an array of applications.

Low-energy synthesis is a consequence of low formation energies in MHPs. The Gibbs free energy of formation ($\Delta_f G°$) is a measure of the thermodynamic driving force for synthesis under standard conditions (25 °C and 1 atm = 101,325 Pa) without external stimuli (e.g., light, heat, H_2O, O_2, etc.). $\Delta_f G°$ is represented by

$$\Delta_f G° = \Delta_f H° - T\Delta_f S° \quad (1)$$

where enthalpy of formation ($\Delta_f H°$) is the energy released or consumed when one mole of a product is synthesized from reactants and can be thought of as a measure of the strength of bonds broken and formed, while entropy of formation ($\Delta_f S°$)

https://doi.org/10.1021/acsenergylett.2c02698
ACS Energy Lett. 2023, 8, 1705−1715

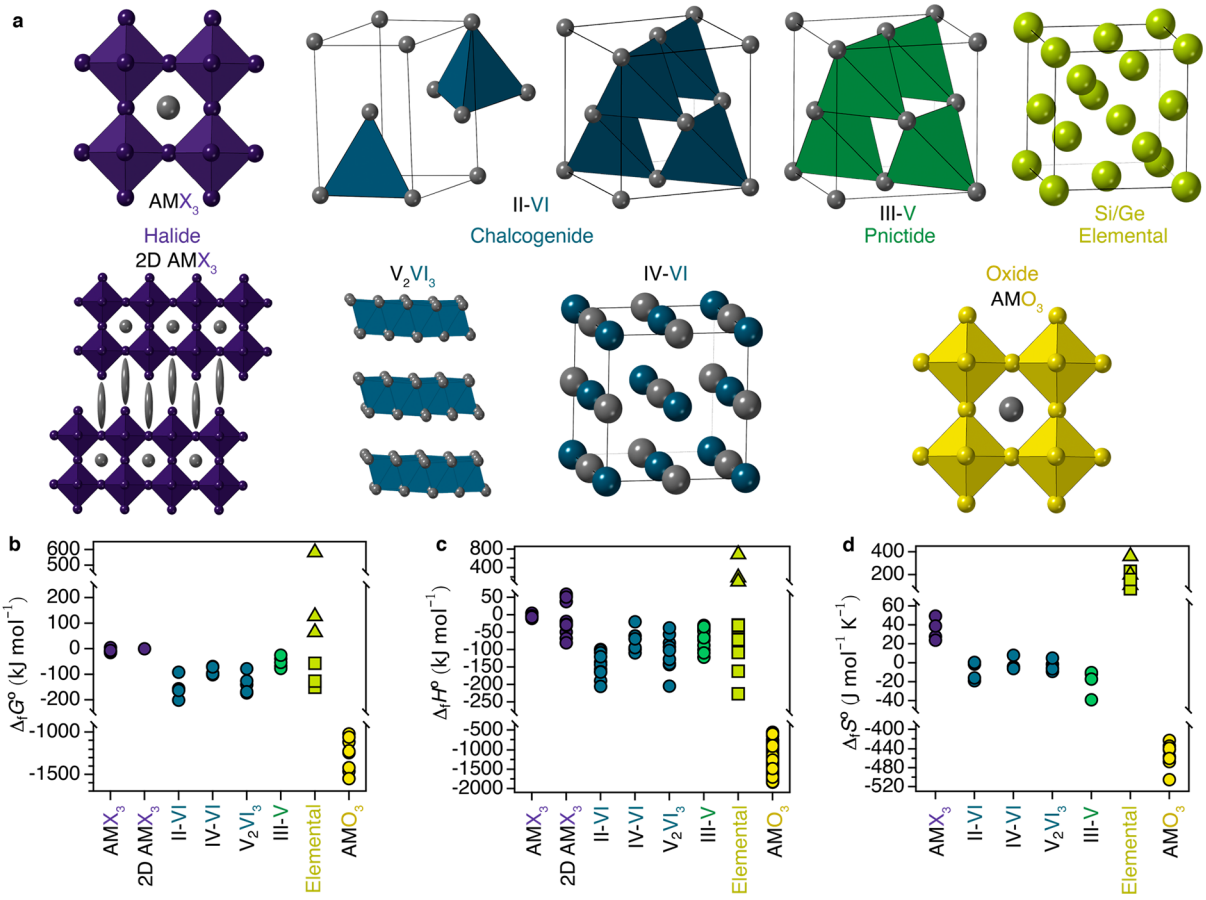

Figure 2. (a) Unit cell comparison of the halide, chalcogenide, pnictide, elemental, and oxide semiconductors compared in this study. Comparison of (b) Gibbs free energy of formation ($\Delta_f G°$), (c) enthalpy of formation ($\Delta_f H°$), and (d) entropy of formation ($\Delta_f S°$) of MHPs to those of other conventional semiconductors. Values for elemental semiconductors were obtained from oxide precursors (triangles) or from chemical vapor deposition (CVD) precursors (squares). Values for chalcogenide, pnictide, and oxide semiconductors were obtained from elemental precursors. Values and literature sources are supplied in Supporting Information.

describes the degree of compositional and energetic disorder in the system. One caveat is that $\Delta_f G°$ values given for standard conditions may vary substantially from the decomposition of materials into binary rather than elemental compounds.

Formation of a compound is thermodynamically favorable for $\Delta_f G° < 0$, and unfavorable for $\Delta_f G° > 0$. We compare the formation energy of MHPs to binary and elemental semiconductors due to their similar applications, with ternary oxide perovskites as a direct structural comparison to MHPs (Figure 2a). MHPs have slightly negative $\Delta_f G°$ values in the range of 0 to −15 kJ mol^{-1}, whereas conventional semiconductors exhibit a large driving force relative to precursors, with deeply negative $\Delta_f G°$ values from −50 to −1500 kJ mol^{-1} (Figure 2b).

The formation energy of inorganic compounds is often discussed in terms of $\Delta_f H°$ due to the inherently strong bonds created when these compounds are formed. Elemental semiconductors prepared by chemical vapor deposition (CVD, squares) as well as binary chalcogenide (II−VI, IV−VI, V_2VI_3) and pnictide (III−V) semiconductors exhibit $\Delta_f H°$ values in the range of −50 to −300 kJ mol^{-1}, whereas ternary oxide perovskites (AMO_3) are as negative as −2000 kJ mol^{-1} (Figure 2c). Large, negative $\Delta_f H°$ values suggest these compounds are unlikely to decompose into precursors due to their strong bonding. Indeed, these compounds are highly stable at >500−1000 °C, leading to their commercial use in challenging environments.[37]

MHPs are typically synthesized from the reaction between alkylammonium or metal halide salts with metal dihalide salts, as described by the following equation:

$$AX + MX_2 \leftrightarrow AMX_3 \quad (2)$$

In contrast to conventional semiconductors, the $\Delta_f H°$ term of MHPs is between +5 and −10 kJ mol^{-1} (Figure 2b), with near-equal driving forces between formation and dissociation into precursors. Resiliency of MHPs to decomposition follows the intuitive trend Cl > Br > I, in agreement with the Pb-halide bond strengths and redox potentials.[38,39] Whereas MHPs are produced from precursors with similar ionic bonds, the precursors for chalcogenide, pnictide, and oxide semiconductors are elemental, metal salts, or organometallics with products containing bonds to metal centers with higher valency anions, resulting in stronger bonding environments.

The $\Delta_f H°$ term typically dominates the $\Delta_f S°$ term in technologically relevant semiconductors due to large, negative $\Delta_f H°$ values and small $\Delta_f S°$ values (0 to −20 J mol^{-1} K^{-1}) (Figure 2d). In contrast, the $\Delta_f S°$ term of MHPs cannot be ignored. MHPs exhibit positive $\Delta_f S°$ (+20 to +60 J mol^{-1} K^{-1}) values that introduce a greater driving force than the near-zero $\Delta_f H°$.[38,40] Entropy is a facile method to improve the operational stability of MHPs in solar cells because $\Delta_f S°$ can be easily increased through alloying and/or doping multiple cations and halides.[12] Despite high susceptibility to decom-

https://doi.org/10.1021/acsenergylett.2c02698
ACS Energy Lett. 2023, 8, 1705−1715

The formation enthalpy term ($\Delta_f H°$) typically dominates the formation entropy term ($\Delta_f S°$) in technologically relevant semiconductors due to large, negative $\Delta_f H°$ values and small $\Delta_f S°$ values (0 to −20 J mol^{-1} K^{-1}). In contrast, the $\Delta_f S°$ term of MHPs cannot be ignored. MHPs exhibit positive $\Delta_f S°$ (+20 to +60 J mol^{-1} K^{-1}) values that introduce a greater driving force than the near-zero $\Delta_f H°$.

position, MHP-based PV devices have maintained >85% of their initial performance after 1000 h[41] of illumination, with the current record at 10,000 h (>1 yr).[42]

The low formation energy of MHPs means small disturbances can lead to decomposition of the MHP into its precursors or transformation into nonperovskite phases. The most widely investigated transformations in MHPs involve H_2O.[43−47] Reversible hydration of MHPs under controlled humidity occurs according to the following reaction:

$$MAPbX_3 + 3MAX + 2H_2O \leftrightarrow MA_4PbX_6{\cdot}2H_2O \quad (3)$$

3D $MAPbI_3$ films prepared with excess MAI (E_G = 1.80 eV) form the 0D hydrated phase $MA_4PbI_6{\cdot}2H_2O$ (λ_{max} = 370 nm = 3.35 eV) above 40% RH and $MAPbI_3$ can be regenerated by dehydrating above 75 °C (Figure 3a).[46] Hydration also causes decomposition of MAX by pushing equilibrium toward volatile MA + HX, forming solid PbI_2 upon leaving the film.[9]

Though detrimental to conventional PV, reversible hydration has been leveraged for applications that benefit from stimuli-responsiveness. For example, switchable PV devices can generate electricity in the colored dehydrated state and offer high light transmittance in a hydrated state,[44,45] which has significant potential to cut building energy use and CO_2 emissions in buildings.[48] In contrast to hydrate phase formation in MA-based MHPs, H_2O triggers reversible dimensionality tuning of Ruddlseden-Popper phases in FA-based MHPs. Whereas most chromic films offer a single-color transition, this mechanism enables switching between multiple colors including yellow, orange, red, brown, and white/colorless by turning the thickness of the layers.[47]

Intercalating species that H-bond with the MHP lattice, including methanol (MeOH),[49] carboxylic acids,[50] and amines,[21,51] can also drive optoelectronic state switching in MHPs. MeOH exhibits weaker H-bonding with the lattice relative to H_2O, reducing switching temperature from 70 to 50 °C. Thermochromic windows utilizing methanolation and PAA have visible transmittance (VT) of 31% in the colored state and 84% in the bleached state, with ∼80% of the initial VT after 200 cycles.[52] Amine vapor transforms the 3D MHP into a lower dimensional MHP through complex formation. This process is reversed at room temperature upon removing the amine vapor (Figure 3a). Sealing the $MAPbI_3{\cdot}xCH_3NH_2$ complex to prevent amine escape enables thermochromic windows that darken upon complex dissociation under solar heating above 60 °C, with a champion PCE of 11.3% and a VT ranging from 3 to 68%.[21]

Polymorphism in MHPs. MHP materials adopt highly symmetric cubic structures at elevated temperatures. Corner-sharing $[MX_6]^{4-}$ octahedra tilt with respect to one another at decreasing temperatures, which results in several polymorphic transitions to lower-symmetry structures (Figure 3a). Polymorphic transformations in MHPs include those that maintain the bonding environment of the original structure but with a change in symmetry, and those that change both the bonding

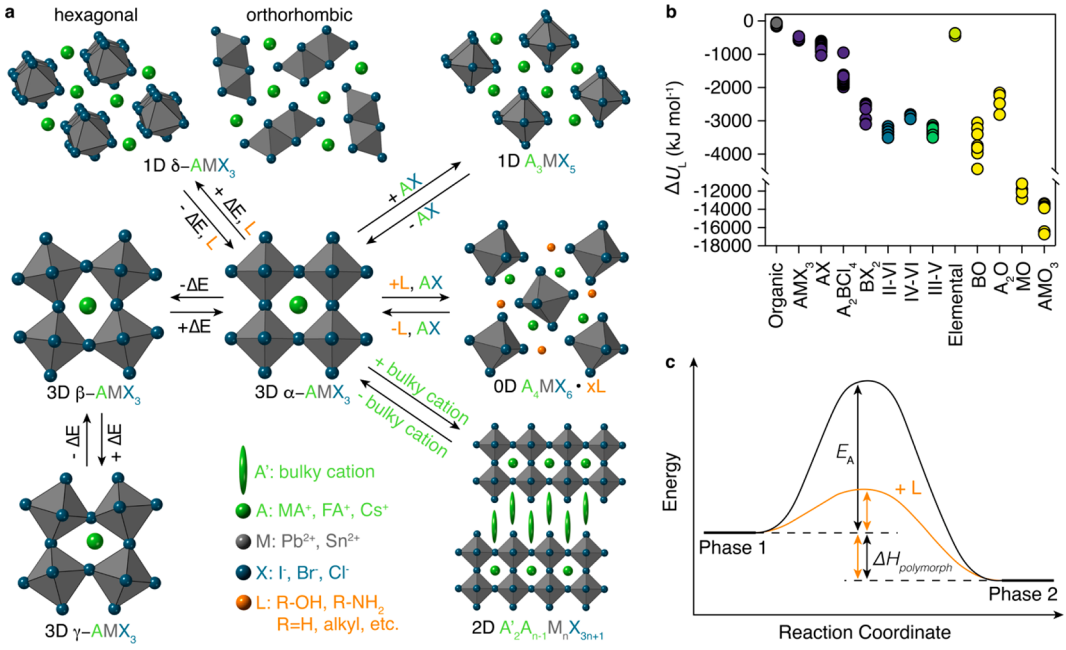

Figure 3. (a) Illustration of transformations between the 3D MHP phase with nonperovskite, low-dimensional 2D, 1D, and 0D structures. (b) Comparison of lattice energy values of MHPs to those of other conventional semiconductors. B is a divalent group II or transition metal. (c) Reaction coordinate diagram describing the thermodynamics of phase transformations in MHPs. The activation energy barrier is decreased upon exposure to an H-bonding molecule (L). Values and literature sources are supplied in Supporting Information.

https://doi.org/10.1021/acsenergylett.2c02698
ACS Energy Lett. 2023, 8, 1705−1715

environment and symmetry. In general, the closer a polymorph is to the original structure, the more similar the optoelectronic properties will be.[53] For example, α (cubic), β (tetragonal), and γ (orthorhombic) polymorphs (Figure 3a) undergo a symmetry change due to octahedral tilting while maintaining a similar bonding environment, resulting in only a 0.2−0.3 eV bandgap difference.[53] MHPs also exhibit two polymorphs near standard conditions with a significant change in bonding environment (3D ↔ 1D) resulting in large differences in optoelectronic properties: a 3D black cubic phase (α, E_G = 1.45−1.75 eV) and a 1D pale-yellow orthorhombic (Cs-based) or hexagonal (FA-based) phase (δ, E_G = 2.40−2.85 eV) (Figure 3a). A comprehensive discussion on the many reversible MHP transformations can be found in ref 31.

The temperature ranges a specific polymorph exists in depends on the composition of the MHP. In general, the temperature range increases from I > Br > Cl, from Pb > Sn, and from FA > Cs > MA, as shown in the table of MA-based polymorph structures in the Supporting Information.[53] Inorganic solids generally exhibit >100 °C temperature differences between polymorphs while organic solids exhibit many polymorphs over smaller temperature ranges (~15 °C).[54] MHPs exhibit small energy differences between polymorphs (5−14 kJ mol^{-1}),[55] comparable to organic materials (<7 kJ mol^{-1}).[56]

Polymorphism reflects lattice energy (ΔU_L), the energy released when infinitely separated ions in the gaseous state under vacuum coalesce to form an ionic lattice. A more negative ΔU_L indicates stronger cohesive forces whereas a near-zero value of ΔU_L indicates a weaker lattice and a small change in energy for transformations to occur. ΔU_L for most ionic semiconductors is significantly larger than the equivalent cohesive energies (ΔU_C) of covalent elemental semiconductors and organic compounds. ΔU_L of binary chalcogenide, pnictide, and oxide compounds is typically in the range of −3000 to −5000 kJ mol^{-1} and up to −18000 kJ mol^{-1} for oxide compounds (Figure 3b). Metal halides compounds (AX, A_2BCl_4, BX_2) exhibit smaller ΔU_L values of −500 to −3500 kJ mol^{-1}. ΔU_L of MHPs is significantly lower than binary chalcogenide, pnictide, and oxide compounds—between 450 to −600 kJ mol^{-1}, calculated from a Born−Haber cycle approach.[69] MHP materials have lattice energies closer to organic compounds or elemental semiconductors than ionic compounds.[57] These lower values of ΔU_L show less energy is needed to form polymorphic crystal structures and suggest the associated phase transitions may also have lower activation energies.

Metal halides compounds (AX, A_2BCl_4, BX_2) exhibit smaller cohesive energy (ΔU_L) values of −500 to −3500 kJ mol^{-1}. ΔU_L of MHPs are closer to organic compounds or elemental semiconductors than ionic compounds.

Beyond the thermodynamic considerations of phase stability, there is also a mechanistic question of how atomic reorganization occurs; if an understanding could be developed at this level, it may encourage new approaches to engineering phase transitions. The mechanistic question is challenging to address experimentally since X-ray and neutron diffraction, for instance, provide spatially and temporally averaged data that primarily reveal the structures of the initial and final phases rather than the local paths of lattice reorganization. Recently, density functional theory and other modeling approaches are beginning to shed light on the nuances of phase transitions, yielding new insights on the role of vacancies, bond strengths, and compositional mixing.[58] Whereas experimental verification of these predictions is challenging, electron microscopy or diffuse X-ray scattering could offer the spatial and temporal resolution required, and the latter has been used to resolve polaron-induced lattice distortion.[59]

Research on conventional applications of MHPs seek to mitigate phase transformations to maintain the desired phase. Though α-phase $MAPbI_3$ launched perovskite PV, FA-rich compositions now yield the highest efficiencies,[60] and Cs-rich compositions are desirable for their thermal stability. α-$CsPbI_3$ and α-$FAPbI_3$ phases are only thermodynamically stable at high temperatures and will spontaneously convert into δ-$CsPbI_3$ and δ-$FAPbI_3$ phases at room temperature on the order of days.

We illustrate polymorphic transformations in MHPs by a reaction coordinate diagram where an activation energy (E_A) barrier must be overcome to transform the original structure (phase 1) into a perovskite or nonperovskite structure (phase 2) with an energy difference of $\Delta H_{polymorph}$ that is small between different MHP polymorphs (Figure 3c). Even the influence of a hydrogen bonding molecules (L) at the crystal surface can induce structural transformations.[30,47] For example, several 2D FA_2PbX_4 polymorphs exist as chains of corner sharing $[PbX_4]^{2-}$ octahedra whose connectivity can vary from (1 × 1), (3 × 2), and (3 × 3) step-like structures in either standard or eclipsed layers with bandgaps only slightly varying within a 0.2 eV range.[61] Because the energy landscape is so shallow, crystallization of a specific polymorph is often kinetically controlled, rather than thermodynamically, where the less energetic phase is trapped by an energy barrier. For instance, a specific polymorph can be obtained by varying the solvent evaporation rate or by exposure to antisolvent.[62] For energetically unfavorable phases, E_A can be increased, mitigating the transition into the favored phase.

$\Delta H_{polymorph}$ can be manipulated by controlling composition, crystal size, or surface chemistry. For example, crystal symmetry breaking in $CsPb(I_{1-x}Br_x)_3$ polymorphs leads to anisotropy in carrier transport, high power factor, and ultralow thermal conductivity resulting in promising thermoelectric figures of merit (ZT) of up to 1.7 at room temperature.[63] Cation vacancies lead to a decrease in the energy difference between the α- and δ-phases.[64] Surface strain introduced by synthesizing <30 nm $CsPbX_3$ quantum dots favors the visibly absorbing α-$CsPbI_3$ phase over the wider bandgap δ-$CsPbI_3$ leading to record PV efficiencies and operational stability for inorganic perovskite PV.[65] Tailored surface chemistry has a similar effect to favor formation of 3D β-$CsPbI_3$ for PV applications,[66] and prevents reaction with the environment.[67] Multiphase films have also found utility with α-$FAPbI_3$ nanocrystals precipitated from δ-$FAPbI_3$ forming a type 1 heterojunction that boosted LED performance by a factor of 58 compared to bulk-$FAPbI_3$ films.[68]

In contrast to efforts to isolate target phases for conventional applications, low-energy polymorphism enables an array of emerging applications. Exposing MHPs to a trigger molecule that H-bonds to the lattice facilitates ionic reorganization by reducing E_A,[30] reducing the transition temperature and

https://doi.org/10.1021/acsenergylett.2c02698
ACS Energy Lett. 2023, 8, 1705−1715

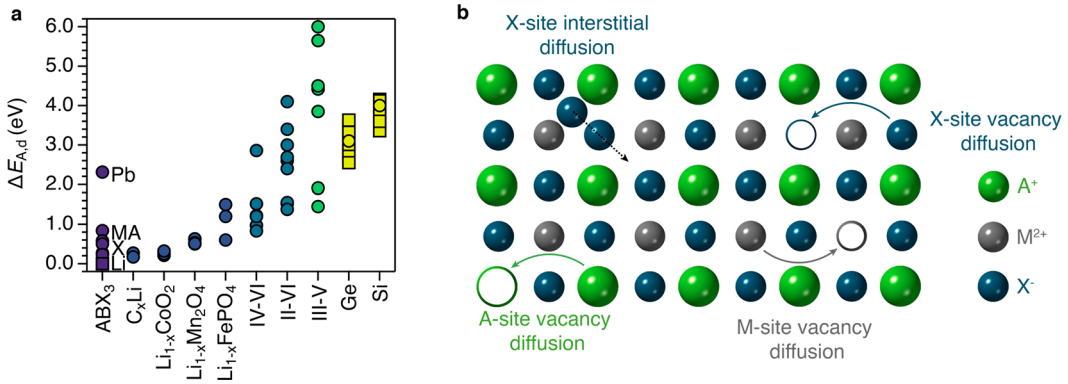

Figure 4. (a) Activation energy of diffusion ($E_{A,d}$) comparison of MHPs to conventional semiconductors and Li-ion battery electrodes. Circles denote intrinsic diffusion and squares denote extrinsic diffusion. (b) Illustration showing the common ion transport mechanisms in MHPs. Values and literature sources are supplied in Supporting Information.

increasing transformation kinetics. These transformations typically require heat to reverse, suggesting E_A is sufficient to prevent spontaneous conversion back to the original phase.[8,69] For instance, the α-to-δ transition is reduced from days to hours upon exposure to humidity, which lowers E_A by initiating ionic reorganization and defect formation at the grain boundary-water interface.[30] The α-phase can be regenerated from the δ-phase upon thermal annealing at high temperatures.[8,69] Thermochromic PV windows that switch between α-$CsPbIBr_2$ (VT = 35.4%, PCE = 4.7%) and δ-$CsPbIBr_2$ (VT = 81.7%, PCE = 0.15%) for over 40 cycles have been fabricated with the α-to-δ transition occurring at 60% RH over 10h and the δ-to-α transition occurring at 150 °C.[30] MHP-based phase change memory (PCM) has been demonstrated by exploiting optoelectronic variability among polymorphs in perovskites exposed to humidity, light, oxygen, and solvents.[70] A 2D MHP exhibited a large shift in the absorption onset between the amorphous (T_m = 173 °C) and crystalline phases (T_c = 101 °C), which may allow for Joule heating PCM and simple device integration, but the electronic properties accompanying this phase change have not yet been investigated.[71]

Ion Transport in MHPs. Mass transport is undesirable for conventional optoelectronic devices because ion transport competes with carrier transport. In PV devices, mobile ion accumulation impacts carrier extraction at the electrical interfaces by screening or permitting the formation of defects that cause nonradiative recombination. Despite these concerns, PVs based on MHPs exhibit comparable PCEs to state-of-the-art PV materials[7] while exhibiting high levels of solid-state ion transport even at room temperature.[72,73] Anomalous properties in MHPs as a result of high ion transport include current–voltage hysteresis, above-bandgap photovoltages, light-induced phase segregation, self-healing, and rapid chemical conversion between cations and anions.[73] Reducing defect density or introducing kinetic barriers to ion transport suppresses ion transport in MHPs, with methods including mixed-cation and mixed-halide alloys,[74] incorporating 2D MHP whose interlayer spacing blocks ion transport,[15] postsynthetic treatment with iodine vapor,[75] doping with K or Rb ions,[76] or exposure to elevated pressure.[13]

The energy input required for ions to migrate throughout a lattice is described by the activation energy of diffusion ($E_{A,d}$) through the following equation:

$$D_{ion} = D_0 e^{(-E_{A,d}/k_B T)} \quad (4)$$

where D_{ion} is the diffusion coefficient of an ion, D_0 is the temperature-independent prefactor, k_B is the Boltzmann constant, and T is the temperature. $E_{A,d}$ can describe both intrinsic diffusion (diffusion of ions that makeup the lattice) and extrinsic diffusion (diffusion of external ions throughout the lattice). Conventional binary and elemental semiconductors typically exhibit intrinsic $E_{A,d}$ values >1.0 eV (Figure 4a, circles); intrinsic ion diffusion is uncommon in these materials. In contrast, MHPs exhibit intrinsic $E_{A,d}$ values <1.0 eV for both the A-site and X-site. The X-site exhibits exceptionally low $E_{A,d}$ values ranging from 0.2 to 0.5 eV, which is on the same order of magnitude as Li^+ diffusion in state-of-the-art Li-ion battery anode (C_xLi) and cathode ($Li_{1-x}ClO_2$, $Li_{1-x}Mn_2O_4$, $Li_{1-x}FePO_4$) electrodes (Figure 4a). These low $E_{A,d}$ values confer remarkable properties such as complete A- and X-site exchange on the order of seconds. The low $E_{A,d}$ values also lead to phase segregation under illumination for mixed MHP compositions, with a driving force provided by the free energy reduction for photocarriers trapped in lower bandgap phases.[13,77] In contrast, the M-site $E_{A,d}$ values are >2.0 eV and therefore remain stationary. MHPs also undergo extrinsic ion diffusion with Li^+ exhibiting $E_{A,d}$ values of ~0.1 eV, compared to 0.5–0.6 eV for Li^+ diffusion in crystalline silicon.[78]

> The X-site exhibits exceptionally low $E_{A,d}$ values ranging from 0.2–0.5 eV, which is on the same order of magnitude as Li^+ diffusion in state-of-the-art Li-ion battery anode (C_xLi) and cathode ($Li_{1-x}ClO_2$, $Li_{1-x}Mn_2O_4$, $Li_{1-x}FePO_4$) electrodes.

Ion transport in MHPs is believed to occur through defects,[73] although direct observations have not indisputably confirmed this, as they have with other material systems.[79] The weak cohesive forces in the MHP lattice lead to high defect concentrations that can even be higher than carrier concentrations.[80] Each of the A-, B-, and X-sites are able to migrate through vacancy-mediated ionic diffusion, and X-sites are also able to migrate interstitially (Figure 4b).[72,73] The corner sharing octahedral network of the MHP lattice gives each ion/vacancy eight nearest neighbors, making vacancy-

https://doi.org/10.1021/acsenergylett.2c02698
ACS Energy Lett. 2023, 8, 1705–1715

mediated ionic diffusion especially prevalent. Low energy input for ions migration is a result of high defect density inherent in MHPs (measured to be 10^{12} cm^{-3} for single crystals, while reliable measurement of thin film defect density has been challenging),[81] many nearest neighbors over short distances, and weak cohesive forces in the lattice.

The high ionic diffusivity of MHPs is suspected to contribute to remarkable radiation hardness, and their high Z elements and long carrier lifetimes make them promising candidates for next-generation radiation detectors.[82] While ionizing radiation can displace nuclei, creating vacancies and trap states, it has been suggested that MHPs "self-heal" as displaced ions diffuse back to lattice sites and restore electronic quality at room temperature.[83] As a result, MHPs have a damage threshold to proton irradiation nearly 3 orders of magnitude higher than crystalline Si, which holds promise for nonterrestrial PV.[83,84] $CsPbBr_3$ also achieved energy resolution of 1.4%,[85] rivaling state-of-the-art cadmium zinc telluride (CZT), and may offer orders of magnitude reduction in cost.[86] Polycrystalline thick film detectors have also been blade coated for direct conversion X-ray imaging.[87] Key challenges remain: single crystals size is limited, electrode diffusion is problematic, high dark currents due to low bulk resistivity and self-doping reduces signal-to-noise ratio, and the spatial resolution of imaging detectors can improve.

High ion transport in MHPs renders them materials of interest for energy storage applications such as Li/Na-ion batteries, photorechargeable batteries, and as solid-state electrolytes.[88] The MHP lattice can be reversibly doped by a variety of ions including Li^+ and Na^+ via electrochemical methods.[89] Li/Na-ion batteries have been fabrication from a variety of MHP compositions including organic, inorganic, 2D, 1D, and transition metals.[88] Notably, low-dimensional perovskites have achieved 646 mAh/g and 961 mAh/g capacities for Li-ion and Na-ion batteries, respectively, exceeding that of conventional graphite anodes (372 mAh/g).[90] The 1D benzidine perovskite cycle life strongly depended on discharge rate, with a worst-case capacity retention of 453 mAh/g after 250 cycles at 500 mA/g. Copper-based 2D MHPs have also been used as Li-ion cathodes with 200 cycles, but their specific capacity was an order of magnitude lower than commercial $LiNiCoMnO_2$ cathodes.[91] MHPs can also undergo color changes upon Li^+ intercalation, and $CsPbBr_3$ electrodes exhibit electrochromism upon Li^+ intercalation between orange and gray/black.[89]

Unlike conventional battery materials, MHP's act as a battery electrode while simultaneously using sunlight to charge itself as a photorechargeable battery. The $Cs_3Pb_2I_9$ defect perovskite demonstrated this effect with a 975 mAh/g capacity under illumination.[92] $MA(Pb/Sn)Cl_3$ has also been used as a solid-state electrolyte, allowing Li-ion transport while suppressing dendrite formation at the surface of Li metal electrodes (specific capacity 3860 mAh/g).[20] Supercapacitors have specific energies 1−2 orders of magnitude greater than conventional electrolytic capacitors (~0.02 Wh/kg) and find a niche where the required charge/discharge rates and cycling life exceed the performance of rechargeable batteries, with applications in regenerative breaking and power grid buffering. 3D $MAPbBr_3$ and 2D PEA_2PbBr_4 supercapacitors, with energy densities up to 9 Wh/kg, retained 98% and ~100%, respectively, of their initial performance after 1,000 charging cycles.[93] Both the energy and power density are comparable to commercial state-of-the-art supercapacitors, but durability testing must be expanded since commercial devices offer 10^6 cycle life. The 3D material offered greater capacitance and energy density, while the improved diffusion kinetics of the 2D material offered greater power density.[94]

High ion transport combined with responsive optoelectronic properties have enabled emerging technologies. Electronic ratchets utilize spatially asymmetric potential distributions to convert nondirectional sources of energy into direct current. Recently, the first MHP electronic ratchet used a voltage stress to redistribute ions within a 2D MHP, converting electronic noise and unbiased square-wave potentials into current.[24] LEC devices induce a p-i-n junction within the MHP layer via ion accumulation at interfaces to enable high emissivity,[25] with advantages over LEDs including simple architecture, cost-efficient fabrication, and air stable electrodes. However, the best LEC $t_{1/2}$ lifetime is 6700 h at 100 cd/m^2, and both the efficiency and lifetimes fall short of commercial LED lighting, which has $t_{1/2}$ lifetimes exceeding 50,000 h.[95] Humidity sensors have also been developed that undergo photoluminescence and resistance changes caused by ion transport induced by exposure to humidity.[96] Control of ion migration through a heterojunction formed between MHP nanocrystals and single-walled carbon nanotubes enables optical switching and functions for neuromorphic computing.[32] Resistive random access memory (ReRAM) utilizes electrochemical metallization to form and rupture metallic filaments, resulting in low and high resistance states. Challenges for MHP-based ReRAM include short retention times (thousands of seconds), low endurance (a few thousand cycles), and insufficient on/off ratios ($<10^{10}$), but these may be overcome. Contracting the lattice by moving from $MAPbI_3$ to $MAPbCl_3$ increased the extrapolated retention time from 1.6 to 28.3 years in a perovskite ReRAM device.[97] The electric field-induced ion migration effect has also been used to reconfigure the photoresponsivity of MHP devices over the range of 540−1270%, which enables the fabrication of adaptive machine vision systems with a maximum 263% enhancement of object recognition accuracy.[98]

SUMMARY AND FUTURE OUTLOOK

The dynamic structural flexibility inherent in metal halide perovskites result from the union of several unique properties whose combination is not observed in other semiconductors. The low formation energies, low energy difference between polymorphs, and high ion transport inherent in MHPs allow its lattice to easily form, break apart, and rearrange with little energy input. Though these features are often problematic for conventional applications, they should not be feared; they offer a unique opportunity to realize emerging applications that require dynamic properties such as switchable PV smart windows, electronic ratchets, solid-state electrolytes, light-emitting electrochemical cells, and memory or neuromorphic computing elements. This work provides a thermodynamic picture of perovskite structural properties and guidance on how to exploit the unique properties. We offer a fresh perspective on the properties of these materials without the PV-centric narrative usually found in the literature.

ASSOCIATED CONTENT

Supporting Information

The Supporting Information is available free of charge at https://pubs.acs.org/doi/10.1021/acsenergylett.2c02698.

https://doi.org/10.1021/acsenergylett.2c02698
ACS Energy Lett. 2023, 8, 1705−1715

Spreadsheet with individual tabs showing values and references for formation energy, lattice energy, and activation energy used in Figures 2−4 and a tab showing space groups of polymorphs of MA-based perovskites (XLSX)

AUTHOR INFORMATION

Corresponding Author

Lance M. Wheeler − *National Renewable Energy Laboratory, Golden, Colorado 80401, United States;* orcid.org/0000-0002-1685-8242; Email: Lance.Wheeler@nrel.gov

Authors

Bryan A. Rosales − *National Renewable Energy Laboratory, Golden, Colorado 80401, United States;* orcid.org/0000-0003-2488-7446

Kelly Schutt − *National Renewable Energy Laboratory, Golden, Colorado 80401, United States*

Joseph J. Berry − *National Renewable Energy Laboratory, Golden, Colorado 80401, United States; Renewable and Sustainable Energy Institute, University of Colorado Boulder, Department of Physics, Boulder, Colorado 80309, United States*

Complete contact information is available at: https://pubs.acs.org/10.1021/acsenergylett.2c02698

Notes

The views expressed in the article do not necessarily represent the views of the DOE or the U.S. Government. The U.S. Government retains and the publisher, by accepting the article for publication, acknowledges that the U.S. Government retains a nonexclusive, paid-up, irrevocable, worldwide license to publish or reproduce the published form of this study, or allow others to do so, for U.S. Government purposes.

The authors declare no competing financial interest.

Biographies

Bryan A. Rosales is a Senior R&D Scientist at Tandem PV and former postdoctoral fellow at the National Renewable Energy Laboratory. He received his Ph.D. from Iowa State University in 2019. His research focuses on solid-state chemistry and scaling perovskite photovoltaics.

Kelly Schutt is a Staff Scientist at the National Renewable Energy Laboratory. He received his Ph.D. from the University of Oxford in 2020. His research is focused on novel perovskite X-ray scintillators and prototyping X-ray detectors for scientific and medical applications. He is also contributing to perovskite photovoltaic research at NREL.

Joseph J. Berry is a Senior Research Fellow at the National Renewable Energy Laboratory. He received his Ph.D. from Penn State University in 2001. He is the perovskite and hybrid solar cells team lead and principal scientist on oxide semiconductor systems, with a focus on basic materials physics and device applications.

Lance M. Wheeler is a Staff Scientist at the National Renewable Energy Laboratory. He received his Ph.D. from the University of Minnesota in 2014. His research focuses on materials chemistry for photovoltaics, next-generation computing, and heat flow applications.

ACKNOWLEDGMENTS

This study was authored by the National Renewable Energy Laboratory, operated by Alliance for Sustainable Energy, LLC, for the U.S. Department of Energy (DOE) under contract No. DEAC36-08GO28308. B.A.R. and L.M.W acknowledges funding provided by the Building Technologies Office within the U.S. Department of Energy Office of Energy Efficiency and Renewable Energy. L.M.W and K.S. acknowledge the Laboratory Directed Research and Development program at the National Renewable Energy Laboratory. J.J.B. acknowledges the Advanced Perovskite Cells and Modules program of the National Center for Photovoltaics, funded by the DOE Office of Energy Efficiency and Renewable Energy, Solar Energy Technologies Office.

REFERENCES

(1) Chouhan, L.; Ghimire, S.; Subrahmanyam, C.; Miyasaka, T.; Biju, V. Synthesis, Optoelectronic Properties and Applications of Halide Perovskites. *Chem. Soc. Rev.* **2020**, *49* (10), 2869−2885. Dey, A.; Ye, J.; De, A.; Debroye, E.; Ha, S. K.; Bladt, E.; Kshirsagar, A. S.; Wang, Z.; Yin, J.; Wang, Y.; et al. State of the Art and Prospects for Halide Perovskite Nanocrystals. *ACS Nano* **2021**, *15* (7), 10775−10981. Fu, Y.; Zhu, H.; Chen, J.; Hautzinger, M. P.; Zhu, X. Y.; Jin, S. Metal Halide Perovskite Nanostructures for Optoelectronic Applications and the Study of Physical Properties. *Nat. Rev. Mater.* **2019**, *4* (3), 169−188. Leijtens, T.; Bush, K. A.; Prasanna, R.; McGehee, M. D. Opportunities and Challenges for Tandem Solar Cells Using Metal Halide Perovskite Semiconductors. *Nat. Energy* **2018**, *3* (10), 828−838. Tennyson, E. M.; Doherty, T. A. S.; Stranks, S. D. Heterogeneity at Multiple Length Scales in Halide Perovskite Semiconductors. *Nat. Rev. Mater.* **2019**, *4* (9), 573−587. Zou, C.; Zhang, C.; Kim, Y.-H.; Lin, L. Y.; Luther, J. M. The Path to Enlightenment: Progress and Opportunities in High Efficiency Halide Perovskite Light-Emitting Devices. *ACS Photon* **2021**, *8* (2), 386−404.

(2) Kim, G. W.; Petrozza, A. Defect Tolerance and Intolerance in Metal-Halide Perovskites. *Adv. Energy Mater.* **2020**, *10* (37), 2001959. Yin, W.-J.; Shi, T.; Yan, Y. Unusual defect physics in $CH_3NH_3PbI_3$ perovskite solar cell absorber. *Appl. Phys. Lett.* **2014**, *104* (6), 063903.

(3) Poindexter, J. R.; Hoye, R. L. Z.; Nienhaus, L.; Kurchin, R. C.; Morishige, A. E.; Looney, E. E.; Osherov, A.; Correa-Baena, J. P.; Lai, B.; Bulovic, V.; et al. High Tolerance to Iron Contamination in Lead Halide Perovskite Solar Cells. *ACS Nano* **2017**, *11* (7), 7101−7109.

(4) Zhu, H.; Miyata, K.; Fu, Y.; Wang, J.; Joshi, P. P.; Niesner, D.; Williams, K. W.; Jin, S.; Zhu, X. Y. Screening in Crystalline Liquids Protects Energetic Carriers in Hybrid Perovskites. *Science* **2016**, *353* (6306), 1409−1413.

(5) Akkerman, Q. A.; Manna, L. What Defines a Halide Perovskite? *ACS Energy Lett.* **2020**, *5* (2), 604−610.

(6) Amerling, E.; Lu, H.; Larson, B. W.; Maughan, A. E.; Phillips, A.; Lafalce, E.; Whittaker-Brooks, L.; Berry, J. J.; Beard, M. C.; Vardeny, Z. V.; et al. A Multi-Dimensional Perspective on Electronic Doping in Metal Halide Perovskites. *ACS Energy Lett.* **2021**, *6* (3), 1104−1123.

(7) *Best Research-Cell Efficiencies Chart*, May 27, 2021. https://www.nrel.gov/pv/cell-efficiency.html (accessed Nov. 21, 2021).

(8) An, Y.; Hidalgo, J.; Perini, C. A. R.; Castro-Méndez, A.-F.; Vagott, J. N.; Bairley, K.; Wang, S.; Li, X.; Correa-Baena, J.-P. Structural Stability of Formamidinium- and Cesium-Based Halide Perovskites. *ACS Energy Lett.* **2021**, *6* (5), 1942−1969.

(9) Boyd, C. C.; Cheacharoen, R.; Leijtens, T.; McGehee, M. D. Understanding Degradation Mechanisms and Improving Stability of Perovskite Photovoltaics. *Chem. Rev.* **2019**, *119* (5), 3418−3451.

(10) Manser, J. S.; Saidaminov, M. I.; Christians, J. A.; Bakr, O. M.; Kamat, P. V. Making and Breaking of Lead Halide Perovskites. *Acc. Chem. Res.* **2016**, *49* (2), 330−338.

(11) Vasileiadou, E. S.; Wang, B.; Spanopoulos, I.; Hadar, I.; Navrotsky, A.; Kanatzidis, M. G. Insight on the Stability of Thick Layers in 2D Ruddlesden-Popper and Dion-Jacobson Lead Iodide Perovskites. *J. Am. Chem. Soc.* **2021**, *143* (6), 2523−2536. Soe, C. M. M.; Nagabhushana, G. P.; Shivaramaiah, R.; Tsai, H.; Nie, W.; Blancon, J. C.; Melkonyan, F.; Cao, D. H.; Traore, B.; Pedesseau, L.; et al. Structural and Thermodynamic Limits of Layer Thickness in 2D Halide Perovskites. *Proc. Natl. Acad. Sci. U. S. A.* **2019**, *116* (1), 58−

66. Liang, C.; Salim, K. M. M.; Li, P.; Wang, Z.; Koh, T. M.; Gu, H.; Wu, B.; Xia, J.; Zhang, Z.; Wang, K.; et al. Controlling the Film Structure by Regulating 2D Ruddlesden−Popper Perovskite Formation Enthalpy for Efficient and Stable Tri-Cation Perovskite Solar Cells. *J. Mater. Chem. A* **2020**, *8* (12), 5874−5881. Quan, L. N.; Yuan, M.; Comin, R.; Voznyy, O.; Beauregard, E. M.; Hoogland, S.; Buin, A.; Kirmani, A. R.; Zhao, K.; Amassian, A.; et al. Ligand-Stabilized Reduced-Dimensionality Perovskites. *J. Am. Chem. Soc.* **2016**, *138*, 2649−2655. Yi, C.; Luo, J.; Meloni, S.; Boziki, A.; Ashari-Astani, N.; Gratzel, C.; Zakeeruddin, S. M.; Rothlisberger, U.; Gratzel, M. Entropic Stabilization of Mixed A-Cation ABX_3 Metal Halide Perovskites for High Performance Perovskite Solar Cells. *Energy Environ. Sci.* **2016**, *9* (2), 656−662.

(12) Kim, S.; Eom, T.; Ha, Y.-S.; Hong, K.-H.; Kim, H. Thermodynamics of Multicomponent Perovskites: A Guide to Highly Efficient and Stable Solar Cell Materials. *Chem. Mater.* **2020**, *32* (10), 4265−4272.

(13) Hutter, E. M.; Muscarella, L. A.; Wittmann, F.; Versluis, J.; McGovern, L.; Bakker, H. J.; Woo, Y.-W.; Jung, Y.-K.; Walsh, A.; Ehrler, B. Thermodynamic Stabilization of Mixed-Halide Perovskites against Phase Segregation. *Cell Rep. Phys. Sci.* **2020**, *1* (8), 100120.

(14) Ono, L. K.; Liu, S. F.; Qi, Y. Reducing Detrimental Defects for High-Performance Metal Halide Perovskite Solar Cells. *Can. J. Chem.* **2020**, *59* (17), 6676−6698.

(15) Zhang, F.; Lu, H.; Tong, J.; Berry, J. J.; Beard, M. C.; Zhu, K. Advances in Two-Dimensional Organic−Inorganic Hybrid Perovskites. *Energy Environ. Sci.* **2020**, *13* (4), 1154−1186.

(16) Chen, Q.; Wu, J.; Ou, X.; Huang, B.; Almutlaq, J.; Zhumekenov, A. A.; Guan, X.; Han, S.; Liang, L.; Yi, Z.; et al. All-Inorganic Perovskite Nanocrystal Scintillators. *Nature* **2018**, *561* (7721), 88−93.

(17) Yu, W.; Li, F.; Yu, L.; Niazi, M. R.; Zou, Y.; Corzo, D.; Basu, A.; Ma, C.; Dey, S.; Tietze, M. L.; et al. Single Crystal Hybrid Perovskite Field-Effect Transistors. *Nat. Commun.* **2018**, *9* (1), 5354.

(18) Kim, Y.-H.; Kim, S.; Kakekhani, A.; Park, J.; Park, J.; Lee, Y.-H.; Xu, H.; Nagane, S.; Wexler, R. B.; Kim, D.-H.; et al. Comprehensive Defect Suppression in Perovskite Nanocrystals for High-Efficiency Light-Emitting Diodes. *Nat. Photonics* **2021**, *15* (2), 148−155.

(19) Christians, J. A.; Schulz, P.; Tinkham, J. S.; Schloemer, T. H.; Harvey, S. P.; Tremolet de Villers, B. J.; Sellinger, A.; Berry, J. J.; Luther, J. M. Tailored Interfaces of Unencapsulated Perovskite Solar Cells for > 1,000 h Operational Stability. *Nat. Energy* **2018**, *3* (1), 68−74.

(20) Yin, Y. C.; Wang, Q.; Yang, J. T.; Li, F.; Zhang, G.; Jiang, C. H.; Mo, H. S.; Yao, J. S.; Wang, K. H.; Zhou, F.; et al. Metal Chloride Perovskite Thin Film Based Interfacial Layer for Shielding Lithium Metal from Liquid Electrolyte. *Nat. Commun.* **2020**, *11* (1), 1761.

(21) Wheeler, L. M.; Moore, D. T.; Ihly, R.; Stanton, N. J.; Miller, E. M.; Tenent, R. C.; Blackburn, J. L.; Neale, N. R. Switchable Photovoltaic Windows Enabled by Reversible Photothermal Complex Dissociation from Methylammonium Lead Iodide. *Nat. Commun.* **2017**, *8* (1), 1722.

(22) Liu, S.; Li, Y.; Wang, Y.; Yu, K. M.; Huang, B.; Tso, C. Y. Near-Infrared-Activated Thermochromic Perovskite Smart Windows. *Adv. Sci. (Weinh)* **2022**, *9* (14), No. e2106090.

(23) Zhang, Q.; Su, R.; Liu, X.; Xing, J.; Sum, T. C.; Xiong, Q. High-Quality Whispering-Gallery-Mode Lasing from Cesium Lead Halide Perovskite Nanoplatelets. *Adv. Funct. Mater.* **2016**, *26* (34), 6238−6245.

(24) Hao, J.; Lu, H.; Nanayakkara, S. U.; Harvey, S. P.; Blackburn, J. L.; Ferguson, A. J. Perovskite Electronic Ratchets for Energy Harvesting. *Adv. Electron. Mater.* **2020**, *6* (12), 2000831.

(25) Gets, D.; Alahbakhshi, M.; Mishra, A.; Haroldson, R.; Papadimitratos, A.; Ishteev, A.; Saranin, D.; Anoshkin, S.; Pushkarev, A.; Danilovskiy, E.; et al. Reconfigurable Perovskite LEC: Effects of Ionic Additives and Dual Function Devices. *Adv. Optical Mater.* **2021**, *9* (3), 2001715.

(26) Hu, S.; Ren, Z.; Djurišić, A. B.; Rogach, A. L. Metal Halide Perovskites as Emerging Thermoelectric Materials. *ACS Energy Lett.* **2021**, *6* (11), 3882−3905.

(27) Han, J. S.; Le, Q. V.; Choi, J.; Kim, H.; Kim, S. G.; Hong, K.; Moon, C. W.; Kim, T. L.; Kim, S. Y.; Jang, H. W. Lead-Free All-Inorganic Cesium Tin Iodide Perovskite for Filamentary and Interface-Type Resistive Switching toward Environment-Friendly and Temperature-Tolerant Nonvolatile Memories. *ACS Appl. Mater. Interfaces* **2019**, *11* (8), 8155−8163.

(28) Cho, H.; Kim, Y. H.; Wolf, C.; Lee, H. D.; Lee, T. W. Improving the Stability of Metal Halide Perovskite Materials and Light-Emitting Diodes. *Adv. Mater.* **2018**, *30* (42), No. e1704587. Zhao, Z.; Gu, F.; Rao, H.; Ye, S.; Liu, Z.; Bian, Z.; Huang, C. Metal Halide Perovskite Materials for Solar Cells with Long-Term Stability. *Adv. Energy Mater.* **2019**, *9* (3), 1802671.

(29) Zhumekenov, A. A.; Saidaminov, M. I.; Mohammed, O. F.; Bakr, O. M. Stimuli-Responsive Switchable Halide Perovskites: Taking Advantage of Instability. *Joule* **2021**, *5* (8), 2027−2046.

(30) Lin, J.; Lai, M.; Dou, L.; Kley, C. S.; Chen, H.; Peng, F.; Sun, J.; Lu, D.; Hawks, S. A.; Xie, C.; et al. Thermochromic Halide Perovskite Solar Cells. *Nat. Mater.* **2018**, *17* (3), 261−267.

(31) Vats, G.; Hodges, B.; Ferguson, A. J.; Wheeler, L. M.; Blackburn, J. L. Optical Memory, Switching, and Neuromorphic Functionality in Metal Halide Perovskite Materials and Devices. *Adv. Mater.* **2022**, No. e2205459.

(32) Hao, J.; Kim, Y.-H.; Habisreutinger, S. N.; Harvey, S. P.; Miller, E. M.; Foradori, S. M.; Arnold, M. S.; Song, Z.; Yan, Y.; Luther, J. M.; et al. Low-Energy Room-Temperature Optical Switching in Mixed-Dimensionality Nanoscale Perovskite Heterojunctions. *Sci. Adv.* **2021**, *7* (18), No. eabf1959.

(33) Chen, H. Two-Step Sequential Deposition of Organometal Halide Perovskite for Photovoltaic Application. *Adv. Funct. Mater.* **2017**, *27* (8), 1605654.

(34) Yao, F.; Peng, J.; Li, R.; Li, W.; Gui, P.; Li, B.; Liu, C.; Tao, C.; Lin, Q.; Fang, G. Room-Temperature Liquid Diffused Separation Induced Crystallization for High-Quality Perovskite Single Crystals. *Nat. Commun.* **2020**, *11* (1), 1194.

(35) Nayak, P. K.; Moore, D. T.; Wenger, B.; Nayak, S.; Haghighirad, A. A.; Fineberg, A.; Noel, N. K.; Reid, O. G.; Rumbles, G.; Kukura, P.; et al. Mechanism for Rapid Growth of Organic-Inorganic Halide Perovskite Crystals. *Nat. Commun.* **2016**, *7*, 13303.

(36) Geisz, J. F.; France, R. M.; Schulte, K. L.; Steiner, M. A.; Norman, A. G.; Guthrey, H. L.; Young, M. R.; Song, T.; Moriarty, T. Six-Junction III−V Solar Cells with 47.1% Conversion Efficiency Under 143 Suns Concentration. *Nat. Energy* **2020**, *5* (4), 326−335.

(37) Nayak, P. K.; Mahesh, S.; Snaith, H. J.; Cahen, D. Photovoltaic Solar Cell Technologies: Analysing the State of the Art. *Nat.Rev. Mater.* **2019**, *4* (4), 269−285. Gorai, P.; McKinney, R. W.; Haegel, N. M.; Zakutayev, A.; Stevanovic, V. A Computational Survey of Semiconductors for Power Electronics. *Energy Environ. Sci.* **2019**, *12* (11), 3338−3347.

(38) Tsvetkov, D. S.; Mazurin, M. O.; Sereda, V. V.; Ivanov, I. L.; Malyshkin, D. A.; Zuev, A. Y. Formation Thermodynamics, Stability, and Decomposition Pathways of $CsPbX_3$ (X = Cl, Br, I) Photovoltaic Materials. *J. Phys. Chem. C* **2020**, *124* (7), 4252−4260.

(39) Kerner, R. A.; Xu, Z.; Larson, B. W.; Rand, B. P. The Role of Halide Oxidation in Perovskite Halide Phase Separation. *Joule* **2021**, *5* (5), 2273. Hang, P.; Xie, J.; Li, G.; Wang, Y.; Fang, D.; Yao, Y.; Xie, D.; Cui, C.; Yan, K.; Xu, J.; et al. An Interlayer with Strong Pb-Cl Bond Delivers Ultraviolet-Filter-Free, Efficient, and Photostable Perovskite Solar Cells. *iScience* **2019**, *21*, 217−227.

(40) Ivanov, I. L.; Steparuk, A. S.; Bolyachkina, M. S.; Tsvetkov, D. S.; Safronov, A. P.; Zuev, A. Y. Thermodynamics of Formation of Hybrid Perovskite-Type Methylammonium Lead Halides. *J. Chem. Thermo* **2018**, *116*, 253−258.

(41) Khenkin, M. V.; Katz, E. A.; Abate, A.; Bardizza, G.; Berry, J. J.; Brabec, C.; Brunetti, F.; Bulović, V.; Burlingame, Q.; Di Carlo, A.; et al. Consensus Statement for Stability Assessment and Reporting for

Perovskite Photovoltaics Based on ISOS Procedures. *Nat. Energy* **2020**, *5* (1), 35−49. Luther, J. M.; Schelhas, L. T. Perovskite solar cells can take the heat. *Science* **2022**, *376* (6588), 28−29. Azmi, R.; Ugur, E.; Seitkhan, A.; Aljamaan, F.; Subbiah, A. S.; Liu, J.; Harrison, G. T.; Nugraha, M. I.; Eswaran, M. K.; Babics, M.; et al. Damp heat stable perovskite solar cells with tailored-dimensionality 2D/3D heterojunctions. *Science* **2022**, *376* (6588), 73−77.

(42) Grancini, G.; Roldan-Carmona, C.; Zimmermann, I.; Mosconi, E.; Lee, X.; Martineau, D.; Narbey, S.; Oswald, F.; De Angelis, F.; Graetzel, M.; et al. One-Year Stable Perovskite Solar Cells by 2D/3D Interface Engineering. *Nat. Commun.* **2017**, *8*, 15684.

(43) Liu, S.; Du, Y. W.; Tso, C. Y.; Lee, H. H.; Cheng, R.; Feng, S. P.; Yu, K. M. Organic Hybrid Perovskite ($MAPbI_{3-x}Cl_x$) for Thermochromic Smart Window with Strong Optical Regulation Ability, Low Transition Temperature, and Narrow Hysteresis Width. *Adv. Funct. Mater.* **2021**, *31*, 2010426. Zhang, Y.; Tso, C. Y.; Iñigo, J. S.; Liu, S.; Miyazaki, H.; Chao, C. Y. H.; Yu, K. M. Perovskite Thermochromic Smart Window: Advanced Optical Properties and Low Transition Temperature. *Appl. Energy* **2019**, *254*, 113690. Koutselas, I. B.; Ducasse, L.; Papavassiliou, G. C. Electronic Properties of Three- and Low-Dimensional Semiconducting Materials with Pb Halide and Sn Halide Units. *J. Phys. Cond. Matter* **1996**, *8* (9), 1217−1227. Vincent, B. R.; Robertson, K. N.; Cameron, T. S.; Knop, O. Alkylammonium Lead Halides. Part 1. Isolated PbI_6^{4-} Ions in $(CH_3NH_3)_4PbI_6{\cdot}2H_2O$. *Can. J. Chem.* **1987**, *65* (5), 1042−1046.

(44) Sharma, S. K.; Phadnis, C.; Das, T. K.; Kumar, A.; Kavaipatti, B.; Chowdhury, A.; Yella, A. Reversible Dimensionality Tuning of Hybrid Perovskites with Humidity: Visualization and Application to Stable Solar Cells. *Chem. Mater.* **2019**, *31* (9), 3111−3117.

(45) Halder, A.; Choudhury, D.; Ghosh, S.; Subbiah, A. S.; Sarkar, S. K. Exploring Thermochromic Behavior of Hydrated Hybrid Perovskites in Solar Cells. *J. Phys. Chem. Lett.* **2015**, *6* (16), 3180−3184.

(46) Huisman, B. A. H.; Palazon, F.; Bolink, H. J. Zero-Dimensional Hybrid Organic-Inorganic Lead Halides and Their Post-Synthesis Reversible Transformation into Three-Dimensional Perovskites. *Inorg. Chem.* **2021**, *60*, 5212−5216.

(47) Rosales, B. A.; Mundt, L. E.; Allen, T. G.; Moore, D. T.; Prince, K. J.; Wolden, C. A.; Rumbles, G.; Schelhas, L. T.; Wheeler, L. M. Reversible Multicolor Chromism in Layered Formamidinium Metal Halide Perovskites. *Nat. Commun.* **2020**, *11* (1), 5234.

(48) Wheeler, V. M.; Kim, J.; Daligault, T.; Rosales, B. A.; Engtrakul, C.; Tenent, R. C.; Wheeler, L. M. Photovoltaic windows cut energy use and CO2 emissions by 40% in highly glazed buildings. *One Earth* **2022**, *5* (11), 1271−1285.

(49) Bamfield, P. *Chromic Phenomena: Technological Applications of Colour Chemistry*; Royal Society of Chemistry: London, 2018.

(50) Wheeler, L. M.; Anderson, N. C.; Bliss, T. S.; Hautzinger, M. P.; Neale, N. R. Dynamic Evolution of 2D Layers Within Perovskite Nanocrystals *via* Salt Pair Extraction and Reinsertion. *J. Phys. Chem. C* **2018**, *122* (25), 14029−14038.

(51) Zhao, T.; Williams, S. T.; Chueh, C.-C.; deQuilettes, D. W.; Liang, P.-W.; Ginger, D. S.; Jen, A. K. Y. Design Rules for the Broad Application of Fast (<1 s) Methylamine Vapor Based, Hybrid Perovskite Post Deposition Treatments. *RSC Adv.* **2016**, *6* (33), 27475−27484. Zhou, Z.; Wang, Z.; Zhou, Y.; Pang, S.; Wang, D.; Xu, H.; Liu, Z.; Padture, N. P.; Cui, G. Methylamine-Gas-Induced Defect-Healing Behavior of $CH_3NH_3PbI_3$ Thin Films for Perovskite Solar Cells. *Angew. Chem., Int. Ed.* **2015**, *54* (33), 9705−9709. Huang, W.; Manser, J. S.; Sadhu, S.; Kamat, P. V.; Ptasinska, S. Direct Observation of Reversible Transformation of $CH_3NH_3PbI_3$ and NH_4PbI_3 Induced by Polar Gaseous Molecules. *J. Phys. Chem. Lett.* **2016**, *7* (24), 5068−5073. Zhao, Y.; Zhu, K. Optical Bleaching of Perovskite $(CH_3NH_3)PbI_3$ Through Room-Temperature Phase Transformation Induced by Ammonia. *Chem. Commun.* **2014**, *50* (13), 1605−1607. Jain, S. M.; Qiu, Z.; Häggman, L.; Mirmohades, M.; Johansson, M. B.; Edvinsson, T.; Boschloo, G. Frustrated Lewis Pair-Mediated Recrystallization of $CH_3NH_3PbI_3$ for Improved Optoelectronic Quality and High Voltage Planar Perovskite Solar Cells. *Energy Environ. Sci.* **2016**, *9* (12), 3770−3782. Kim, S.-H.; Kirakosyan, A.; Choi, J.; Kim, J. H. Detection of Volatile Organic Compounds (VOCs), Aliphatic Amines, Using Highly Fluorescent Organic-Inorganic Hybrid Perovskite Nanoparticles. *Dyes Pigm* **2017**, *147*, 1−5.

(52) Rosales, B. A.; Kim, J.; Wheeler, V. M.; Crowe, L. E.; Prince, K. J.; Mirzokarimov, M.; Daligault, T.; Duell, A.; Wolden, C. A.; Schelhas, L. T.; Wheeler, L. M. Thermochromic Metal Halide Perovskite Windows with Ideal Transition Temperatures. *Adv. Energy Mater.* **2023**, 2203331.

(53) Alaei, A.; Circelli, A.; Yuan, Y.; Yang, Y.; Lee, S. S. Polymorphism in Metal Halide Perovskites. *Mater. Adv.* **2021**, *2* (1), 47−63.

(54) Sun, W.; Dacek, S. T.; Ong, S. P.; Hautier, G.; Jain, A.; Richards, W. D.; Gamst, A. C.; Persson, K. A.; Ceder, G. The Thermodynamic Scale of Inorganic Crystalline Metastability. *Sci. Adv.* **2016**, *2* (11), No. e1600225.

(55) Wang, B.; Novendra, N.; Navrotsky, A. Energetics, Structures, and Phase Transitions of Cubic and Orthorhombic Cesium Lead Iodide ($CsPbI_3$) Polymorphs. *J. Am. Chem. Soc.* **2019**, *141* (37), 14501−14504. Zhao, X.-G.; Dalpian, G. M.; Wang, Z.; Zunger, A. Polymorphous Nature of Cubic Halide Perovskites. *Phys. Rev. B* **2020**, *101* (15), 155137.

(56) Nyman, J.; Day, G. M. Static and Lattice Vibrational Energy Differences Between Polymorphs. *CrystEngComm* **2015**, *17* (28), 5154−5165.

(57) Zheng, C.; Rubel, O. Ionization Energy as a Stability Criterion for Halide Perovskites. *J. Phys. Chem. C* **2017**, *121* (22), 11977−11984.

(58) Jiang, J.; Liu, F.; Tranca, I.; Shen, Q.; Tao, S. Atomistic and Electronic Origin of Phase Instability of Metal Halide Perovskites. *ACS Appl. Energy Mater.* **2020**, *3* (12), 11548−11558.

(59) Guzelturk, B.; Winkler, T.; Van de Goor, T. W. J.; Smith, M. D.; Bourelle, S. A.; Feldmann, S.; Trigo, M.; Teitelbaum, S. W.; Steinruck, H. G.; de la Pena, G. A.; et al. Visualization of dynamic polaronic strain fields in hybrid lead halide perovskites. *Nat. Mater.* **2021**, *20* (5), 618−623.

(60) Jeong, J.; Kim, M.; Seo, J.; Lu, H.; Ahlawat, P.; Mishra, A.; Yang, Y.; Hope, M. A.; Eickemeyer, F. T.; Kim, M.; et al. Pseudo-Halide Anion Engineering for Alpha-$FAPbI_3$ Perovskite Solar Cells. *Nature* **2021**, *592* (7854), 381−385.

(61) Guo, Y.; Elliott, C.; McNulty, J.; Cordes, D.; Slawin, A.; Lightfoot, P. New Variants of (110)-Oriented Layered Lead Bromide Perovskites, Templated by Formamidinium or Pyrazolium. *Eur. J. Inorg. Chem.* **2021**, *2021*, 3404−3411.

(62) Fateev, S. A.; Petrov, A. A.; Marchenko, E. I.; Zubavichus, Y. V.; Khrustalev, V. N.; Petrov, A. V.; Aksenov, S. M.; Goodilin, E. A.; Tarasov, A. B. FA_2PbBr_4: Synthesis, Structure, and Unusual Optical Properties of Two Polymorphs of Formamidinium-Based Layered (110) Hybrid Perovskite. *Chem. Mater.* **2021**, *33* (5), 1900−1907.

(63) Yan, L.; Wang, M.; Zhai, C.; Zhao, L.; Lin, S. Symmetry Breaking Induced Anisotropic Carrier Transport and Remarkable Thermoelectric Performance in Mixed Halide Perovskites $CsPb(I_{1-x}Br_x)_3$. *ACS Appl. Mater. Interfaces* **2020**, *12* (36), 40453−40464.

(64) Kye, Y.-H.; Yu, C.-J.; Jong, U.-G.; Ri, K.-C.; Kim, J.-S.; Choe, S.-H.; Hong, S.-N.; Li, S.; Wilson, J. N.; Walsh, A. Vacancy-Driven Stabilization of the Cubic Perovskite Polymorph of $CsPbI_3$. *J. Phys. Chem. C* **2019**, *123* (15), 9735−9744.

(65) Yuan, J.; Hazarika, A.; Zhao, Q.; Ling, X.; Moot, T.; Ma, W.; Luther, J. M. Metal Halide Perovskites in Quantum Dot Solar Cells: Progress and Prospects. *Joule* **2020**, *4* (6), 1160−1185. Kong, X.; Zong, K.; Lee, S. S. Nanoconfining Optoelectronic Materials for Enhanced Performance and Stability. *Chem. Mater.* **2019**, *31* (14), 4953−4970.

(66) Wang, Y.; Dar, M. I.; Ono, L. K.; Zhang, T.; Kan, M.; Li, Y.; Zhang, L.; Wang, X.; Yang, Y.; Gao, X.; et al. Thermodynamically Stabilized β-$CsPbI_3$−Based Perovskite Solar Cells with Efficiencies > 18%. *Science* **2019**, *365* (6453), 591−595.

(67) Moot, T.; Dikova, D. R.; Hazarika, A.; Schloemer, T. H.; Habisreutinger, S. N.; Leick, N.; Dunfield, S. P.; Rosales, B. A.; Harvey, S. P.; Pfeilsticker, J. R.; et al. Beyond Strain: Controlling the

https://doi.org/10.1021/acsenergylett.2c02698
ACS Energy Lett. 2023, 8, 1705−1715

Surface Chemistry of CsPbI3 Nanocrystal Films for Improved Stability against Ambient Reactive Oxygen Species. *Chem. Mater.* **2020**, *32* (18), 7850−7860.
(68) Lee, D.-K.; Shin, Y.; Jang, H. J.; Lee, J.-H.; Park, K.; Lee, W.; Yoo, S.; Lee, J. Y.; Kim, D.; Lee, J.-W.; et al. Nanocrystalline Polymorphic Energy Funnels for Efficient and Stable Perovskite Light-Emitting Diodes. *ACS Energy Lett.* **2021**, *6* (5), 1821−1830.
(69) Masi, S.; Gualdrón-Reyes, A. F.; Mora-Seró, I. Stabilization of Black Perovskite Phase in $FAPbI_3$ and $CsPbI_3$. *ACS Energy Lett.* **2020**, *5* (6), 1974−1985.
(70) Minh, D. N.; Nguyen, L. A. T.; Trinh, C. T.; Oh, C.; Eom, S.; Vu, T. V.; Choi, J.; Sim, J. H.; Lee, K. G.; Kim, J.; et al. Low-Dimensional Single-Cation Formamidinium Lead Halide Perovskites ($FA_{m+2}Pb_mBr_{3m+2}$): From Synthesis to Rewritable Phase-Change Memory Film. *Adv. Funct. Mater.* **2021**, *31* (17), 2011093. Zou, C.; Zheng, J.; Chang, C.; Majumdar, A.; Lin, L. Y. Nonvolatile Rewritable Photomemory Arrays Based on Reversible Phase-Change Perovskite for Optical Information Storage. *Adv. Optical Mater.* **2019**, *7* (18), 1900558.
(71) Singh, A.; Jana, M. K.; Mitzi, D. B. Reversible Crystal-Glass Transition in a Metal Halide Perovskite. *Adv. Mater.* **2021**, *33* (3), No. e2005868.
(72) Moia, D.; Maier, J. Ion Transport, Defect Chemistry, and the Device Physics of Hybrid Perovskite Solar Cells. *ACS Energy Lett.* **2021**, *6* (4), 1566−1576.
(73) Walsh, A.; Stranks, S. D. Taking Control of Ion Transport in Halide Perovskite Solar Cells. *ACS Energy Lett.* **2018**, *3* (8), 1983−1990.
(74) Kim, J. Y.; Lee, J. W.; Jung, H. S.; Shin, H.; Park, N. G. High-Efficiency Perovskite Solar Cells. *Chem. Rev.* **2020**, *120* (15), 7867−7918.
(75) Zohar, A.; Levine, I.; Gupta, S.; Davidson, O.; Azulay, D.; Millo, O.; Balberg, I.; Hodes, G.; Cahen, D. What Is the Mechanism of $MAPbI_3$ p-Doping by I_2? Insights from Optoelectronic Properties. *ACS Energy Lett.* **2017**, *2* (10), 2408−2414.
(76) Abdi-Jalebi, M.; Andaji-Garmaroudi, Z.; Cacovich, S.; Stavrakas, C.; Philippe, B.; Richter, J. M.; Alsari, M.; Booker, E. P.; Hutter, E. M.; Pearson, A. J.; et al. Maximizing and Stabilizing Luminescence from Halide Perovskites with Potassium Passivation. *Nature* **2018**, *555* (7697), 497−501. Saliba, M.; Matsui, T.; Domanski, K.; Seo, J.-Y.; Ummadisingu, A.; Zakeeruddin, S. M.; Correa-Baena, J.-P.; Tress, W. R.; Abate, A.; Hagfeldt, A.; et al. Incorporation of Rubidium Cations into Perovskite Solar Cells Improves Photovoltaic Performance. *Science* **2016**, *354* (6309), 206.
(77) Chen, Z.; Brocks, G.; Tao, S.; Bobbert, P. A. Unified Theory for Light-Induced Halide Segregation in Mixed Halide Perovskites. *Nat. Commun.* **2021**, *12* (1), 2687.
(78) Choi, Y. S.; Park, J. H.; Ahn, J. P.; Lee, J. C. Interfacial Reactions in the Li/Si diffusion couples: Origin of Anisotropic Lithiation of Crystalline Si in Li-Si batteries. *Sci. Rep* **2017**, *7* (1), 14028. Canham, L. T. *Properties of Silicon, Electronic Materials Information Service (EMIS)*; INSPEC, 1988.
(79) Ishikawa, R.; Mishra, R.; Lupini, A. R.; Findlay, S. D.; Taniguchi, T.; Pantelides, S. T.; Pennycook, S. J. Direct observation of dopant atom diffusion in a bulk semiconductor crystal enhanced by a large size mismatch. *Phys. Rev. Lett.* **2014**, *113* (15), 155501. Zhang, J.; Roth, N.; Tolborg, K.; Takahashi, S.; Song, L.; Bondesgaard, M.; Nishibori, E.; Iversen, B. B. Direct observation of one-dimensional disordered diffusion channel in a chain-like thermoelectric with ultralow thermal conductivity. *Nat. Commun.* **2021**, *12* (1), 6709.
(80) Walsh, A.; Scanlon, D. O.; Chen, S.; Gong, X. G.; Wei, S. H. Self-Regulation Mechanism for Charged Point Defects in Hybrid Halide Perovskites. *Angew. Chem., Int. Ed.* **2015**, *54* (6), 1791−1794.
(81) Siekmann, J.; Ravishankar, S.; Kirchartz, T. Apparent Defect Densities in Halide Perovskite Thin Films and Single Crystals. *ACS Energy Lett.* **2021**, *6* (9), 3244−3251.
(82) Zhou, Y.; Chen, J.; Bakr, O. M.; Mohammed, O. F. Metal Halide Perovskites for X-ray Imaging Scintillators and Detectors. *ACS Energy Lett.* **2021**, *6* (2), 739−768.
(83) Lang, F.; Nickel, N. H.; Bundesmann, J.; Seidel, S.; Denker, A.; Albrecht, S.; Brus, V. V.; Rappich, J.; Rech, B.; Landi, G.; et al. Radiation Hardness and Self-Healing of Perovskite Solar Cells. *Adv. Mater.* **2016**, *28* (39), 8726−8731.
(84) Yang, S.; Xu, Z.; Xue, S.; Kandlakunta, P.; Cao, L.; Huang, J. Organohalide Lead Perovskites: More Stable than Glass Under Gamma-Ray Radiation. *Adv. Mater.* **2019**, *31* (4), No. e1805547.
(85) He, Y.; Petryk, M.; Liu, Z.; Chica, D. G.; Hadar, I.; Leak, C.; Ke, W.; Spanopoulos, I.; Lin, W.; Chung, D. Y.; et al. $CsPbBr_3$ Perovskite Detectors with 1.4% Energy Resolution for High-Energy γ-Rays. *Nat. Photonics* **2021**, *15* (1), 36−42.
(86) Wei, H.; Huang, J. Halide Lead Perovskites for Ionizing Radiation Detection. *Nat. Commun.* **2019**, *10* (1), 1066.
(87) Kim, Y. C.; Kim, K. H.; Son, D. Y.; Jeong, D. N.; Seo, J. Y.; Choi, Y. S.; Han, I. T.; Lee, S. Y.; Park, N. G. Printable Organometallic Perovskite Enables Large-Area, Low-Dose X-ray Imaging. *Nature* **2017**, *550* (7674), 87−91.
(88) Zhang, L.; Miao, J.; Li, J.; Li, Q. Halide Perovskite Materials for Energy Storage Applications. *Adv. Funct. Mater.* **2020**, *30* (40), 2003653.
(89) Jiang, Q.; Chen, M.; Li, J.; Wang, M.; Zeng, X.; Besara, T.; Lu, J.; Xin, Y.; Shan, X.; Pan, B.; et al. Electrochemical Doping of Halide Perovskites with Ion Intercalation. *ACS Nano* **2017**, *11* (1), 1073−1079.
(90) Tathavadekar, M.; Krishnamurthy, S.; Banerjee, A.; Nagane, S.; Gawli, Y.; Suryawanshi, A.; Bhat, S.; Puthusseri, D.; Mohite, A. D.; Ogale, S. Low-Dimensional Hybrid Perovskites as High Performance Anodes for Alkali-Ion Batteries. *J. Mater. Chem. A* **2017**, *5* (35), 18634−18642.
(91) Jaffe, A.; Karunadasa, H. I. Lithium Cycling in a Self-Assembled Copper Chloride-Polyether Hybrid Electrode. *Inorg. Chem.* **2014**, *53* (13), 6494−6496.
(92) Tewari, N.; Shivarudraiah, S. B.; Halpert, J. E. Photo-rechargeable Lead-Free Perovskite Lithium-Ion Batteries Using Hexagonal $Cs_3Bi_2I_9$ Nanosheets. *Nano Lett.* **2021**, *21* (13), 5578−5585.
(93) Zhao, J.; Burke, A. F. Review on supercapacitors: Technologies and performance evaluation. *J. Energy Chem.* **2021**, *59*, 276−291.
(94) Kumar, R.; Bag, M. Quantifying Capacitive and Diffusion-Controlled Charge Storage from 3D Bulk to 2D Layered Halide Perovskite-Based Porous Electrodes for Efficient Supercapacitor Applications. *J. Phys. Chem. C* **2021**, *125* (31), 16946−16954.
(95) Gao, J. Polymer light-emitting electrochemical cells—Recent advances and future trends. *Current Opinion in Electrochemistry* **2018**, *7*, 87−94.
(96) Cho, M. Y.; Kim, S.; Kim, I. S.; Kim, E. S.; Wang, Z. J.; Kim, N. Y.; Kim, S. W.; Oh, J. M. Perovskite-Induced Ultrasensitive and Highly Stable Humidity Sensor Systems Prepared by Aerosol Deposition at Room Temperature. *Adv. Funct. Mater.* **2020**, *30* (3), 1907449. Weng, Z.; Qin, J.; Umar, A. A.; Wang, J.; Zhang, X.; Wang, H.; Cui, X.; Li, X.; Zheng, L.; Zhan, Y. Lead-Free $Cs_2BiAgBr_6$ Double Perovskite-Based Humidity Sensor with Superfast Recovery Time. *Adv. Funct. Mater.* **2019**, *29* (24), 1902234. Xu, W.; Li, F.; Cai, Z.; Wang, Y.; Luo, F.; Chen, X. An Ultrasensitive and Reversible Fluorescence Sensor of Humidity Using Perovskite $CH_3NH_3PbBr_3$. *J. Mater. Chem. C* **2016**, *4* (41), 9651−9655.
(97) Zhang, Y.; Poddar, S.; Huang, H.; Gu, L.; Zhang, Q.; Zhou, Y.; Yan, S.; Zhang, S.; Song, Z.; Huang, B.; et al. Three-Dimensional Perovskite Nanowire Array-Based Ultrafast Resistive RAM with Ultralong Data Retention. *Sci. Adv.* **2021**, *7* (36), No. eabg3788.
(98) Chen, Q.; Zhang, Y.; Liu, S.; Han, T.; Chen, X.; Xu, Y.; Meng, Z.; Zhang, G.; Zheng, X.; Zhao, J.; et al. Switchable Perovskite Photovoltaic Sensors for Bioinspired Adaptive Machine Vision. *Adv. Intell. Syst.* **2020**, *2* (9), 2000122.

https://doi.org/10.1021/acsenergylett.2c02698
ACS Energy Lett. 2023, 8, 1705−1715